Supporting Information

Symmetrical-waveform alternating current-promoted NiO$_x$H$_y$ electrocatalysis for oxygen evolution reaction

Zhihao Qi,[a] Jinwei Zhuang, [a] Wantong Yang, [a] Yonggang Yang, [a] Ling Wang, [a] Chenyang Cai, [a] Zhilin Zhang, [a] Yutao Hua, [a] Dilnur Abdirazik, [a] Longhua Li, [a] Weidong Shi*[a] and Jinhui Hao*[a]

[a.] School of Chemistry and Chemical Engineering, Jiangsu University, Zhenjiang, China

*Corresponding authors

*E-mail: swd1978@ ujs.edu.cn; jinhu1_hao@ujs.edu.cn

EXPERIMENTAL SECTION

Materials

Ethanol (AR, 99.7%), potassium hydroxide (KOH, GR), and nickel nitrate hexahydrate ($Ni(NO_3)_2 \cdot 6H_2O$) were purchased from Sinopharm Chemical Reagent Co. Sodium hydroxide (NaOH, AR) was purchased from Nanjing Chemical Reagent Co. The carbon paper was purchased from Shanghai Hesen Electric Co. The thickness of the carbon paper is 0.20 mm.

Synthesis of NiO

Carbon paper (2 cm × 2.5 cm) was pretreated by ultrasonic in ethanol and deionized water for 20 min, respectively. 30 mL of 0.5 M $Ni(NO_3)_2$ solution was added to the electrolytic cell, where Ag/AgCl, carbon paper, and glassy carbon were used as the reference, working, and counter electrode, respectively. Electrodeposition was performed at an applied potential of -1.5 V for 100 s. The carbon paper was rinsed with deionized water and dried to obtain the precursors. The precursor was placed in a tube furnace and heated up to 400 °C at a heating rate of 10 °C/min at atmospheric pressure, and held at this temperature for 60 min and cooled to room temperature to obtain the NiO catalyst. The NiO was pre-scanned with LSV technique until the current response stable. This process enables the fully oxidation of surface structure and the obtained electrocatalyst was denoted as NiO_xH_y.

Synthesis of NiO_xH_y-AC-X

In the three-electrode system, Hg/HgO, NiO_xH_y and glassy carbon were used as the reference, working and counter electrodes, respectively. During the SW-AC process, the action time of each potential was 5 s, and the total treatment time was 20 min, during which 120 AC potential cycles were employed.

In situ Raman measurement of NiO_xH_y-AC-X

In the in situ Raman electrolytic cell, Hg/HgO, NiO_xH_y and glass carbon were used as the reference electrode, working electrode and counter electrode, respectively. The working electrode was employed SW-AC with a small frequency of 0.2 Hz. After activation for 20 min, Raman signal was collected under positive or negative potential of SW-AC with interval of 5 s.

Characterizations

X-ray diffraction (XRD) was performed on Smartlab9 to obtain the crystal structure of the electrocatalyst. Scanning electron microscope (SEM) images were recorded in a Hitachi S-4800 cold field emission scanning electron microscope. Transmission electron microscopy (TEM) and high-resolution transmission electron microscopy (HRTEM) were performed using the TECNAI G2 transmission electron microscope. Electrocatalysts were measured on A300-10/12 for electron paramagnetic resonance (EPR) spectroscopy. X-ray photoelectron spectroscopy (XPS) analysis was performed using Escalab 250Xi. Raman spectroscopy was performed using a QE Pro spectrometer.

Electrochemical Measurements

The electrochemical measurements were performed on CHI 660E workstation with the prepared electrocatalyst sample as the working electrode, glass carbon as the counter electrode and Hg/HgO as the reference electrode, respectively. A 30 mm diameter proton exchange membrane with a thickness of 183 μm was used to separate the anodic and cathodic. 1 M KOH was purified to remove the trace Fe and used as electrolyte. Cyclic voltammetry (CV) was performed for 20 cycles to obtain a stable current response before recording the data. Linear sweep voltammetry (LSV) curves at a scan rate of 10 mv s^{-1} were collected. The EIS data were tested at an applied potential of 0.65 V (vs. Hg/HgO) with a frequency range of 10^{-2} - 10^6 Hz. The distribution of relaxation times (DRT) was calculated from the EIS data according to the reported method.[1]

The difference in the content of internal and external charges on the active surface of the electrocatalyst can be calculated according to the method in the literature.[2] The total surface charge (q_T) is related with the total active surface of the electrocatalyst. q_T can be divided into inner charge (q_I) and outer charge (q_O). The calculation formula is as follow:

$$\frac{1}{q_v} = \frac{1}{q_T} + k_1 v^{1/2}$$

where v is the scan rate, q_v is the charge measured by the CV curve at scan rate v, k_1 is a constant.

By plotting $1/q_v$ vs $v^{1/2}$, the q_T can be obtained.

$$q_v = q_O + k_2 v^{-1/2}$$

where k_2 is a constant.

By plotting q_v vs $v^{-1/2}$, the q_O can be obtained.

The effective diffusion coefficient (D_{eff}) of the active species is calculated from the Nernst-Einstein equation.[3] The λ^0_m can be calculated from the solution resistance (R_s) and the physical dimensions of electrodes. The EIS data were measured at applied potential of 0.02 V (vs. Hg/HgO), frequency range was chosen from 1-10^4 Hz.

The apparent activation energy (E_{app}) of the electrocatalyst can be calculated from electrochemical tests at different temperatures, and the relationship between current density and apparent activation energy can be expressed by Arrhenius equation:

$$j = A_{app}\,exp\!\left(-\frac{E_{app}}{RT}\right)$$

where j is current density in the CV curve, A_{app} is exponential prefactor, E_{app} is apparent activation energy, R is ideal gas constant, and T is temperature during the CV test.

E_{app} was calculated according to the following equation:[4]

$$\left|\frac{\partial(log_{10}j)}{\partial 1/T}\right|_\eta = -\frac{E_{app}}{2.303\,R}$$

where η is overpotential.

DFT calculation

DFT calculation was realized by using the Vienna Ab initio Simulation Package (VASP).[5] Perdew-Burke-Ernzerh (RPBE) within the generalized-gradient approximation (GGA) was used to describe the exchange-correlation energy.[6, 7] The Monkhorst-Pack grids for constructed model was set to 9×9×1. The thickness of the vacuum layer was set to 20 Å.
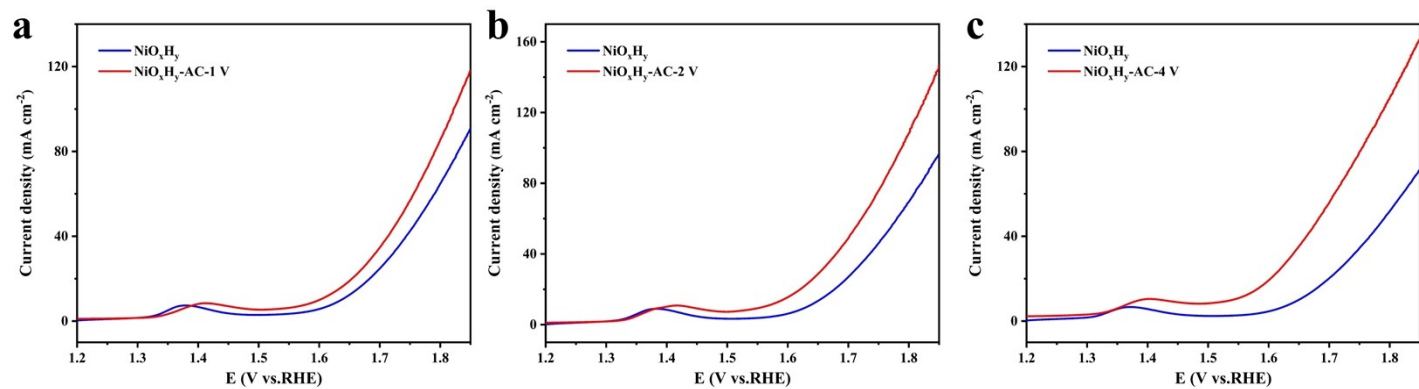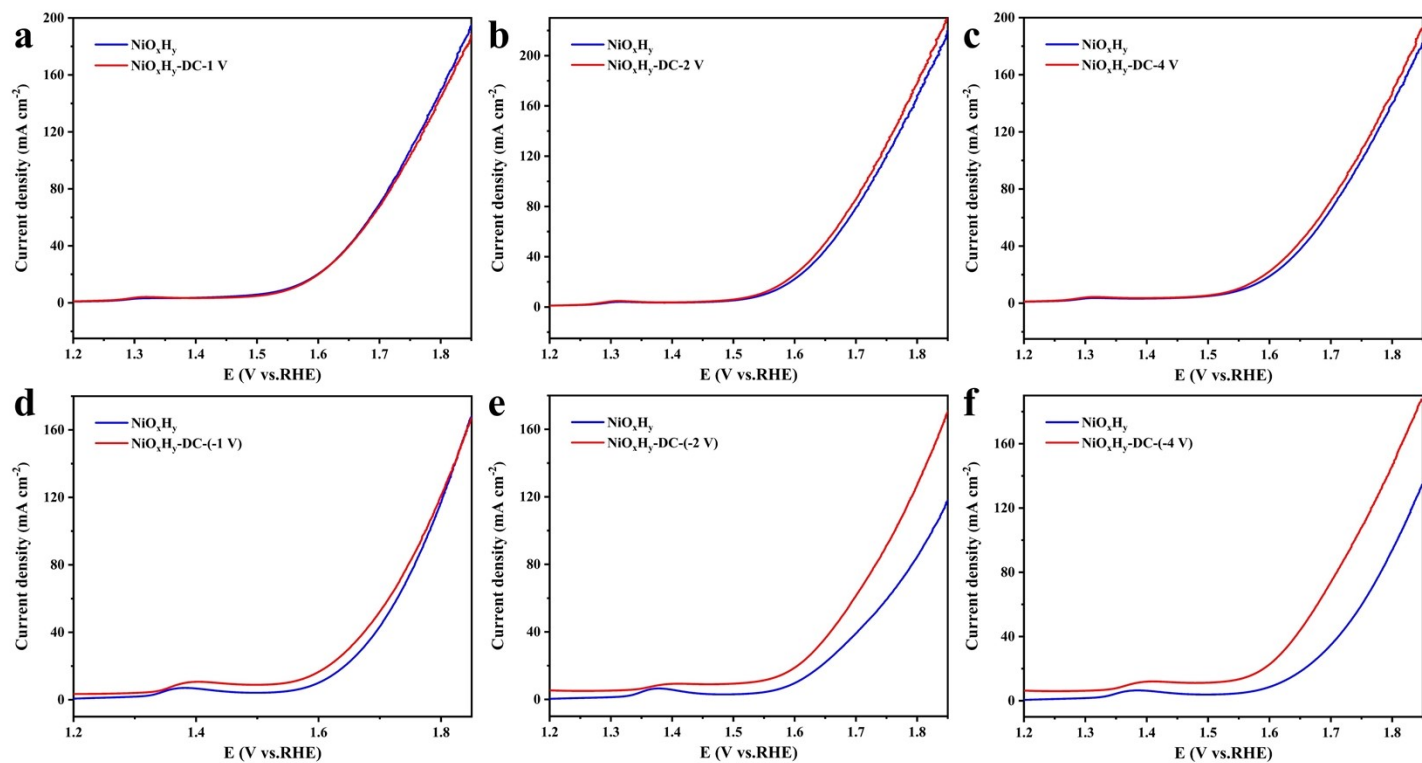
Fig. S1 LSV curves of NiO_xH_y and NiO_xH_y-AC-X. (a) NiO_xH_y-AC-1 V. (b) NiO_xH_y-AC-2 V. (c) NiO_xH_y-AC-4 V.
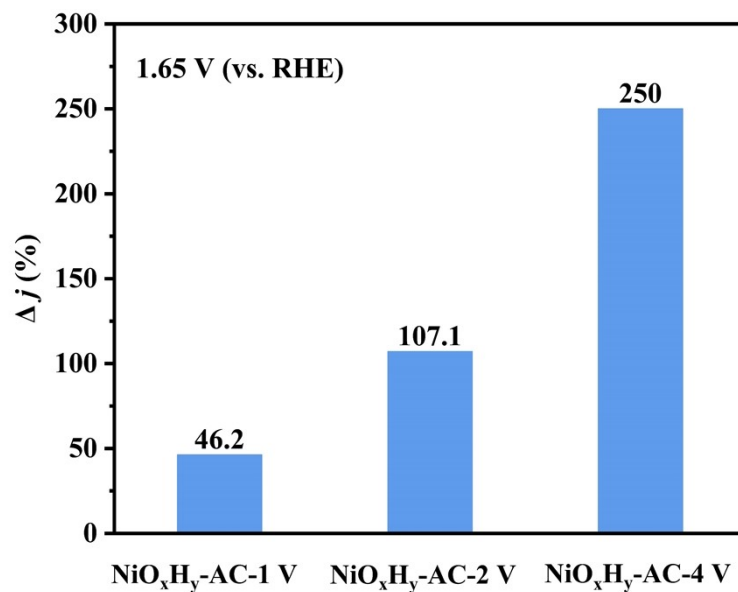
Fig. S2 Percentage of current density difference (Δj) after activation of different potential at the onset potential.
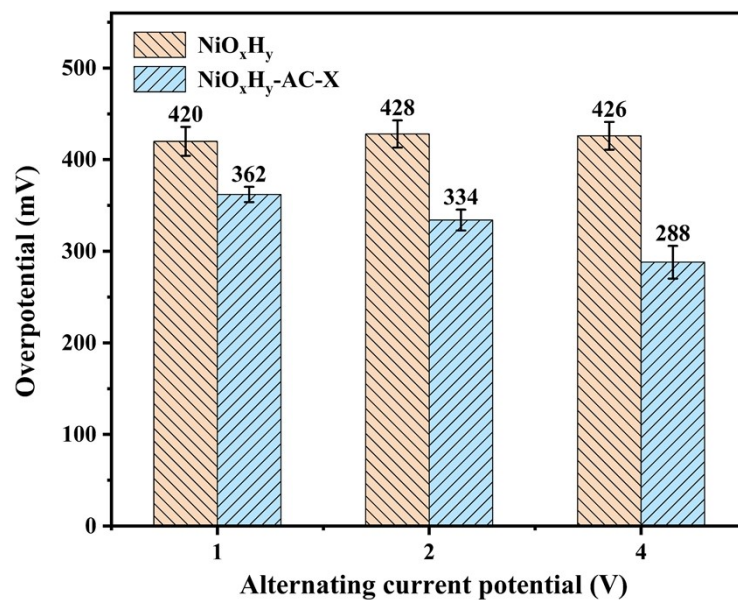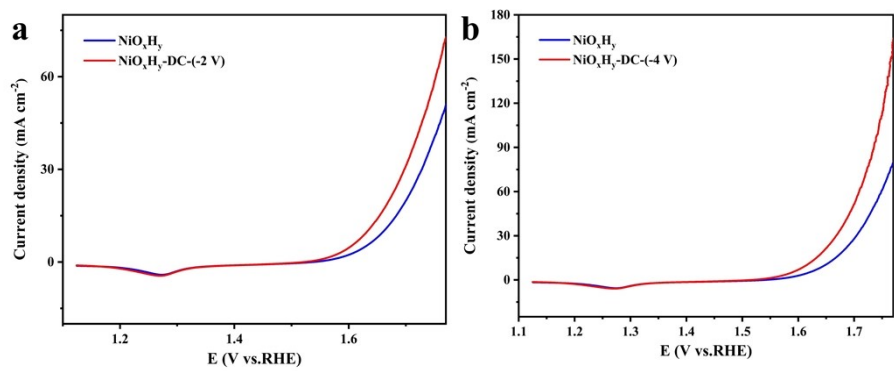
Fig. S3 Variety of overpotential to achieve the current density of 10 mA cm^{-2} before and after SW-AC activation.
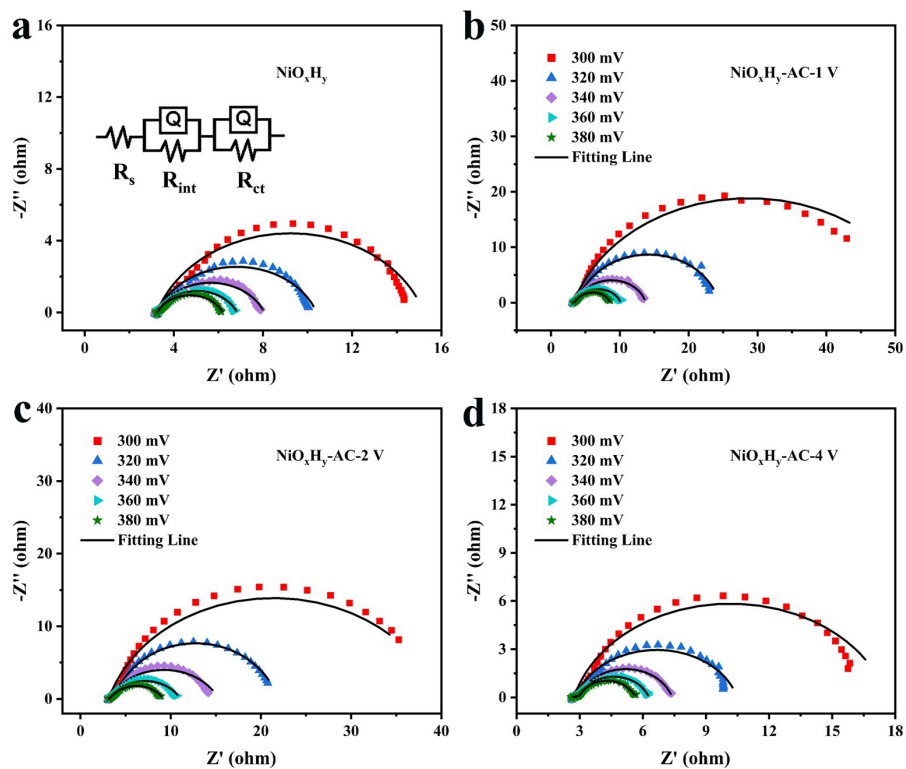
Fig. S4 Influence of direct current (DC) activation on the LSV performance. (a) NiO$_x$H$_y$-DC-1 V. (b) NiO$_x$H$_y$-DC-2 V. (c) NiO$_x$H$_y$-DC-4 V. (d) NiO$_x$H$_y$-DC-(-1 V). (e) NiO$_x$H$_y$-DC-(-2 V). (f) NiO$_x$H$_y$-DC-(-4 V).
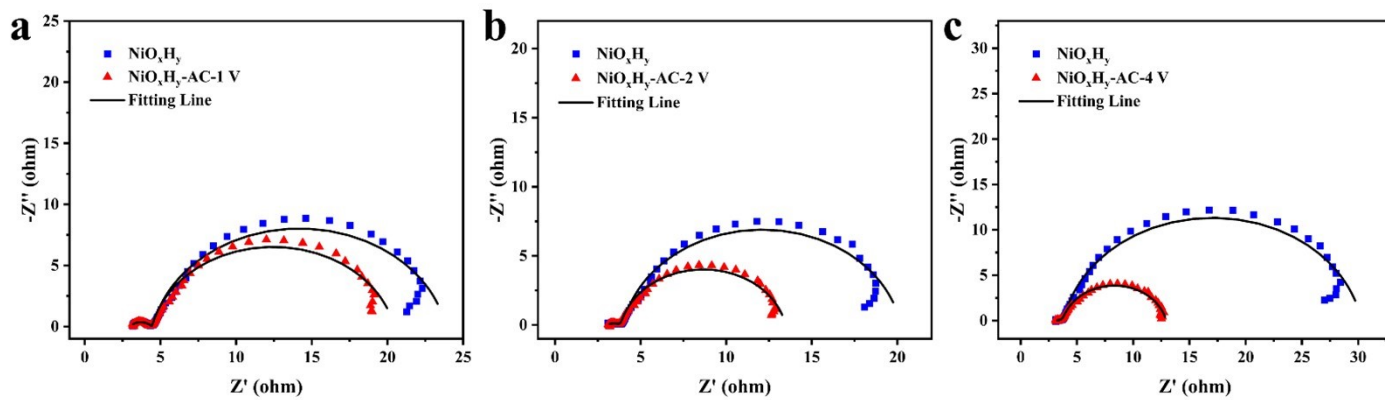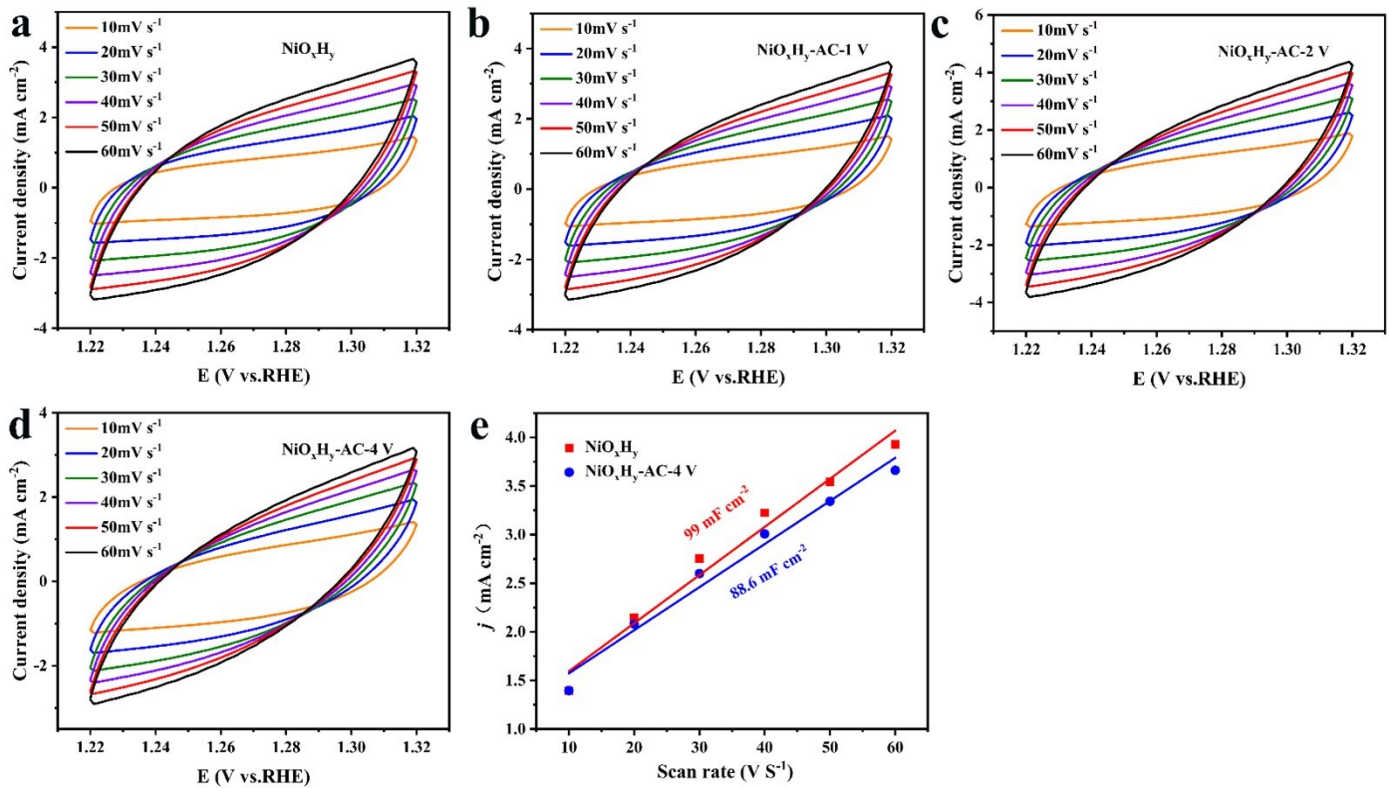
Fig. S5 Reverse scan LSV curves of (a) NiO_xH_y-DC-(-2 V). (b) NiO_xH_y-DC-(-4 V).

Fig. S6 Nyquist plots at multiple overpotentials. (a) NiO$_x$H$_y$. (b) NiO$_x$H$_y$-AC-1 V. (c) NiO$_x$H$_y$-AC-2 V. (d) NiO$_x$H$_y$-AC-4 V. The inset of (a) shows the two-constant equivalent circuit for simulation.

Fig. S7 Nyquist plots of NiO$_x$H$_y$ and NiO$_x$H$_y$-AC-X. (a) NiO$_x$H$_y$-AC-1 V. (b) NiO$_x$H$_y$-AC-2 V.

Fig. S8 CV curves of NiO$_x$H$_y$ and NiO$_x$H$_y$-AC-X. (a) NiO$_x$H$_y$. (b) NiO$_x$H$_y$-AC-1V. (c) NiO$_x$H$_y$-AC-2 V. (d) NiO$_x$H$_y$-AC-4 V. (e)

Correlation between current density difference (Δj) and scan rate at applied potential of 1.27 V.
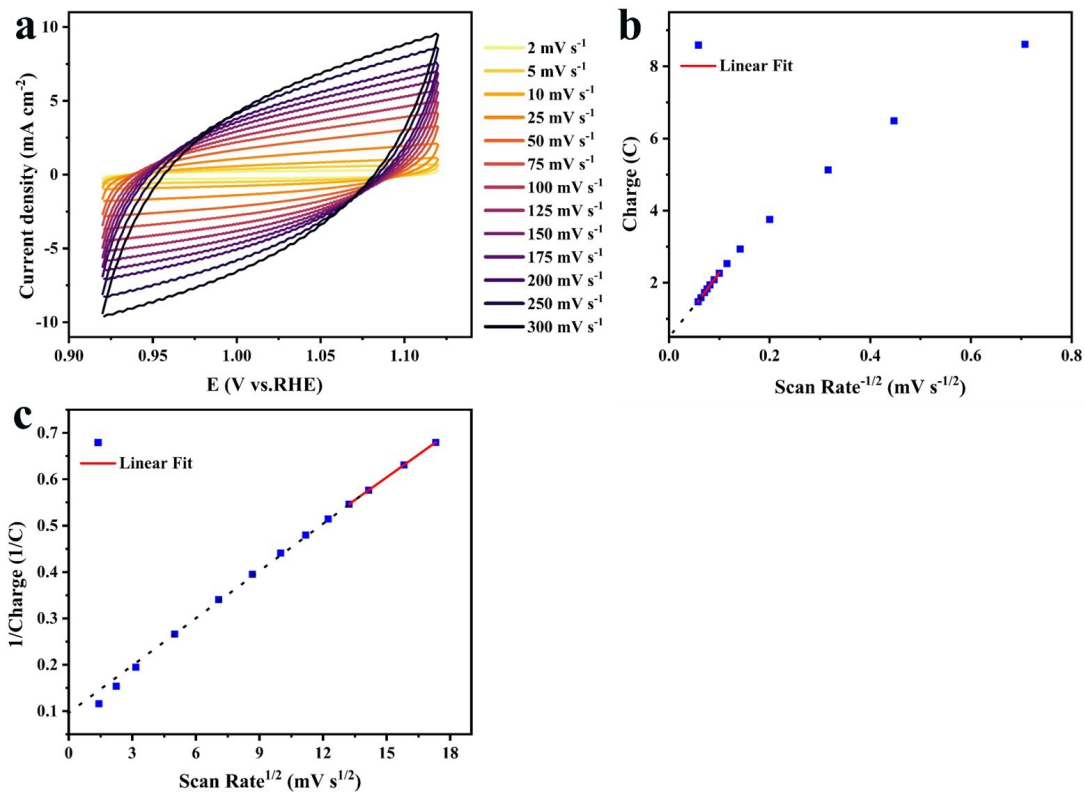
Fig. S9 (a) CV curves for calculating the q_T and q_O. (b) Charge plotted against the scan rate$^{-1/2}$, the intercept of the y-axis in fitting curve is calculated to be q_O. (c) 1/charge plotted against the scan rate$^{1/2}$, the y-axis 1/intercept in fitting curve is calculated to be q_T.
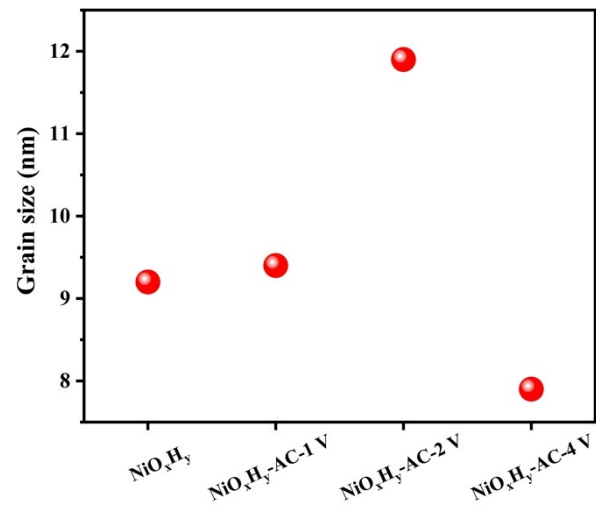
Fig. S10 The grain size diagram of NiO_xH_y and NiO_xH_y-AC-X.
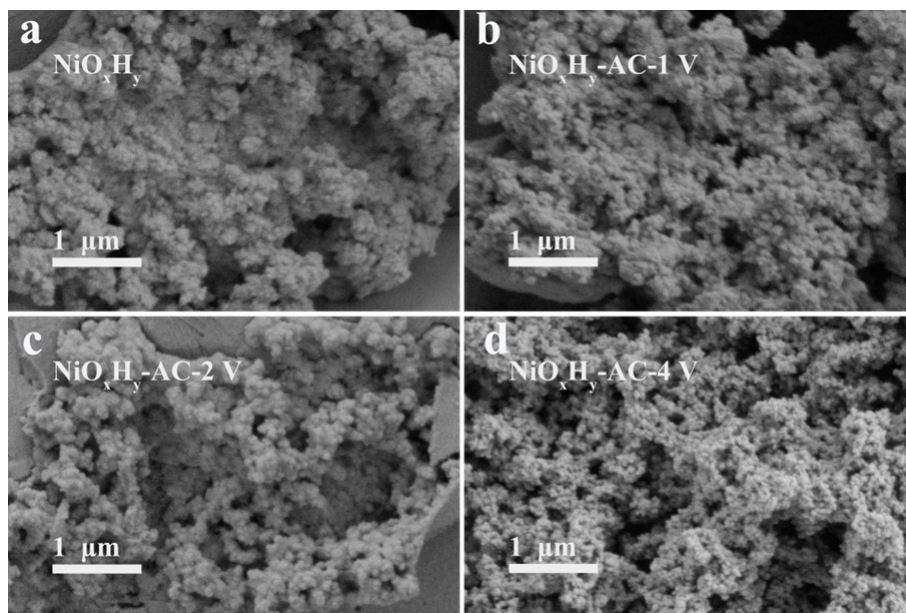
Fig. S11 SEM image of NiO$_x$H$_y$ (a), NiO$_x$H$_y$-AC-1 V (b), NiO$_x$H$_y$-AC-2 V (c), and NiO$_x$H$_y$-AC-4 V (d).
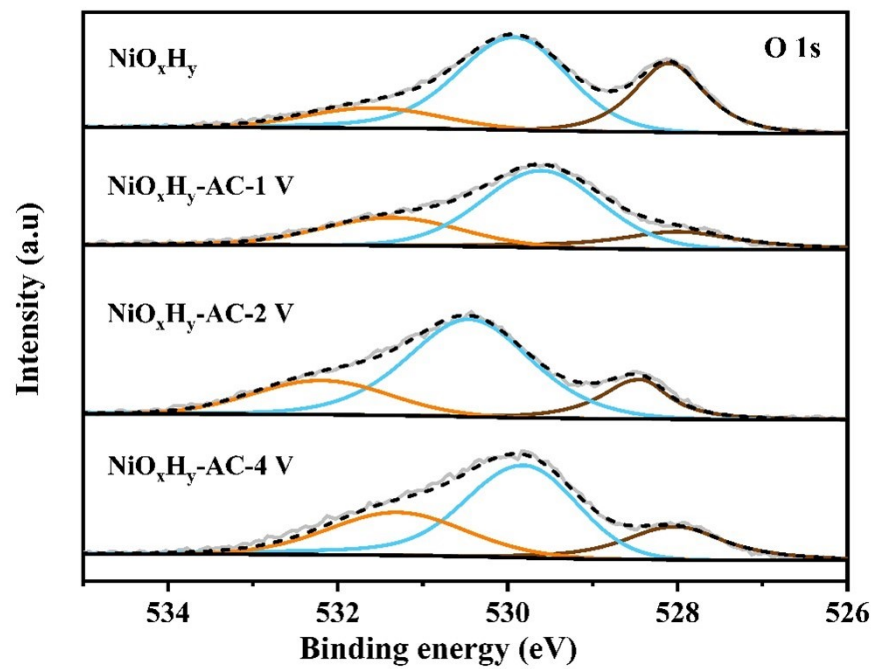
Fig. S12 O 1S XPS spectra of NiO$_x$H$_y$ and NiO$_x$H$_y$-AC-X.
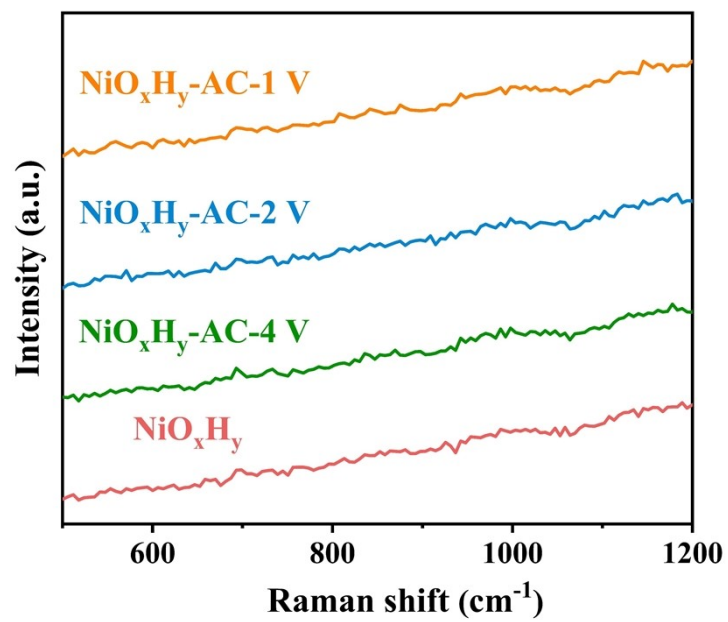
Fig. S13 In situ Raman spectra of NiO_xH_y and NiO_xH_y-AC-X collected at negative potential of SW-AC.
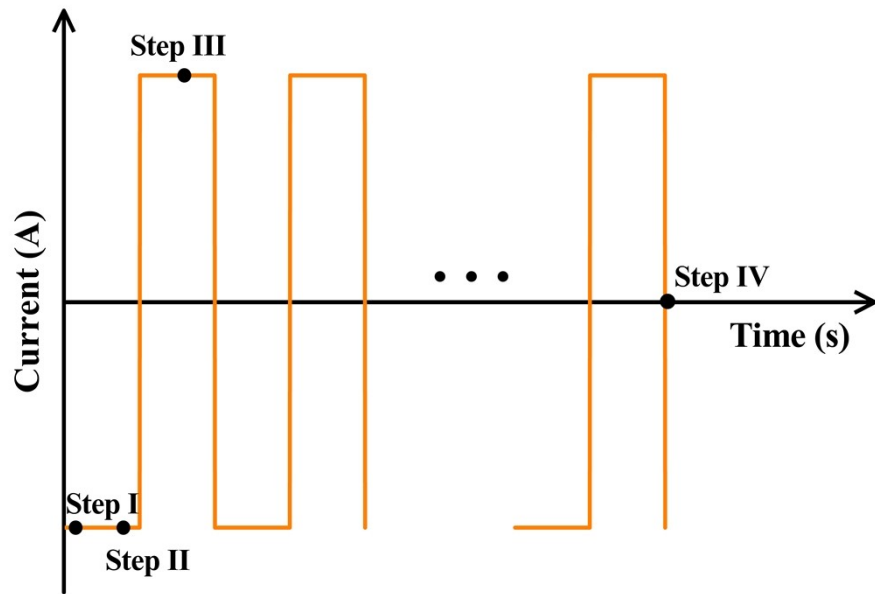
Fig. S14 Illustration of i-t curve during SW-AC activation.
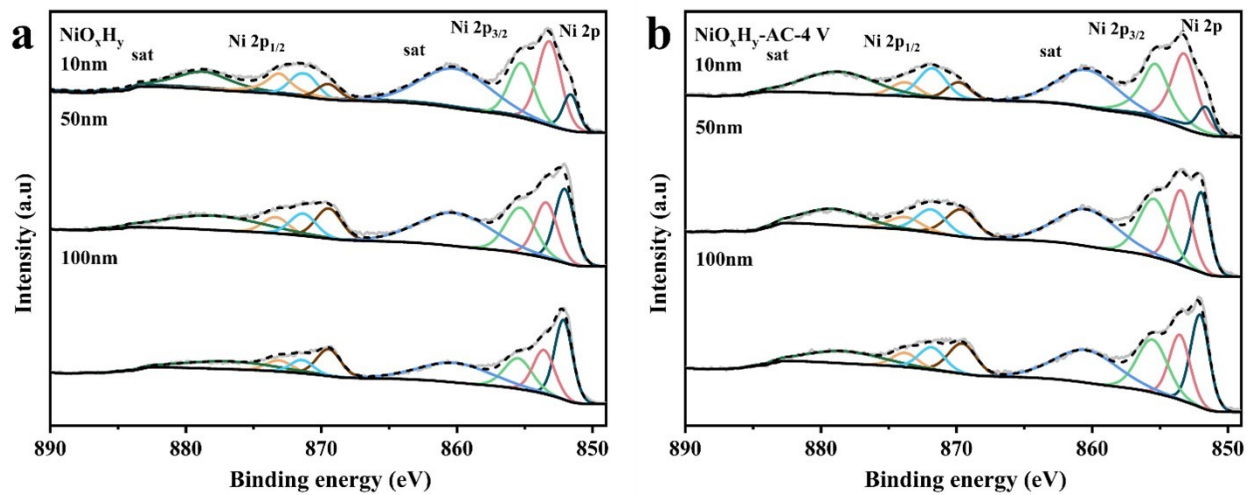
Fig. S15 Ni 2p XPS at different etching degree of NiO_xH_y (a) and NiO_xH_y-AC-4V (b).
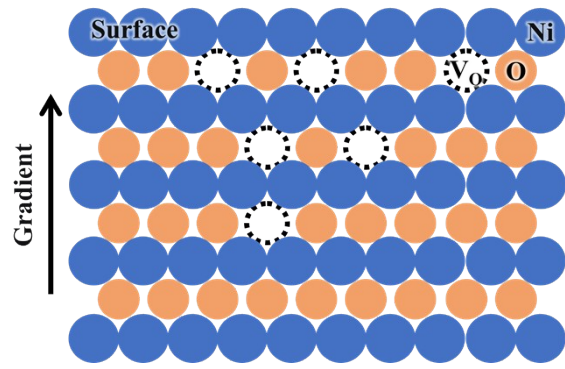
Fig. S16 V_O distribution diagram of NiO_xH_y-AC-4V.
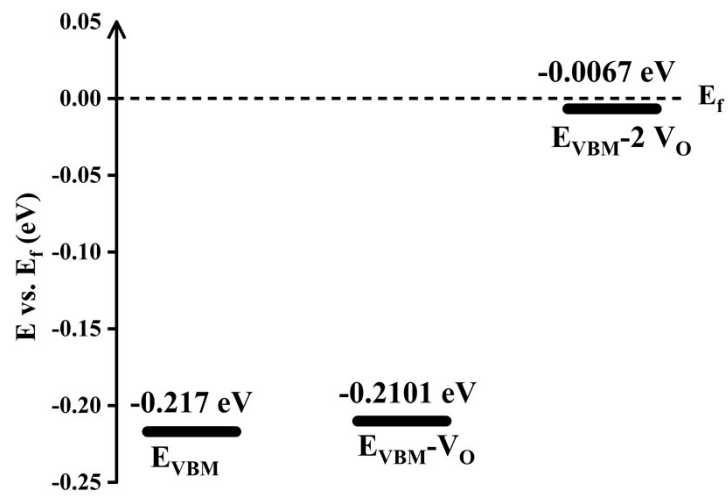
Fig. S17 E_{VBM} of NiO_xH_y, NiO_xH_y-V_O, and NiO_xH_y-$2V_O$.
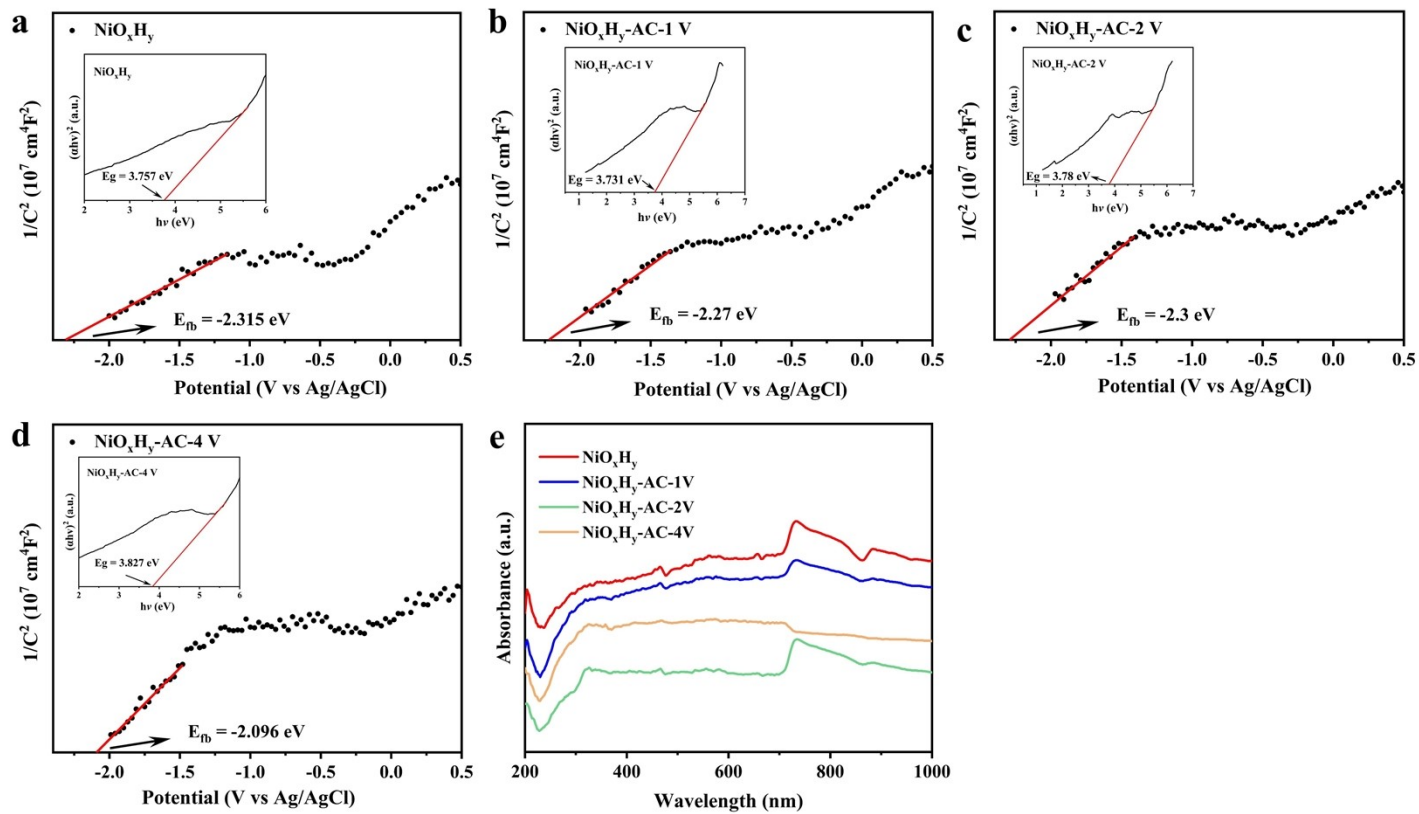
Fig. S18 Mott-Schottky plots of (a) NiO$_x$H$_y$. (b) NiO$_x$H$_y$-AC-1. (c) NiO$_x$H$_y$-AC-2 V. (d) NiO$_x$H$_y$-AC-4 V and the inset is Eg diagram. (e) UV–vis DRS spectra of. NiO$_x$H$_y$ and NiO$_x$H$_y$-AC-X.
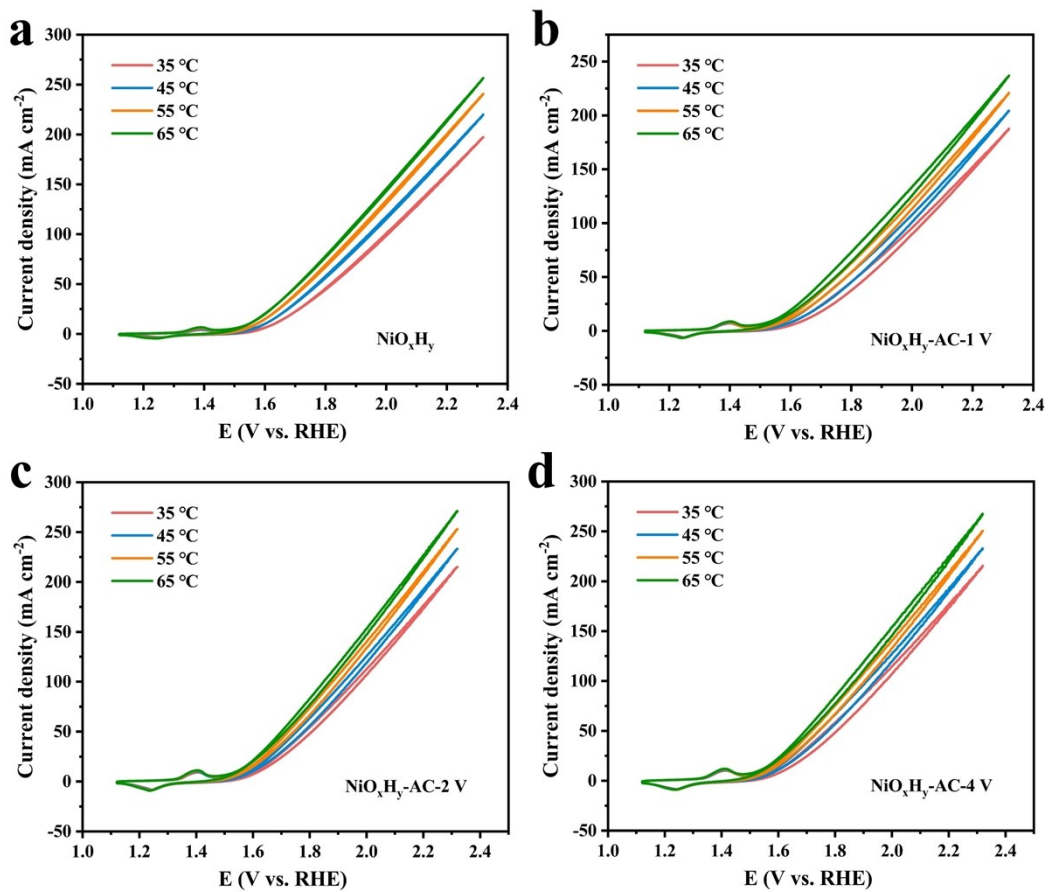
Fig. S19 CV curves of NiO$_x$H$_y$ (a), NiO$_x$H$_y$-AC-1V (b), NiO$_x$H$_y$-AC-2V (c) and NiO$_x$H$_y$-AC-4V (d) at different temperatures.
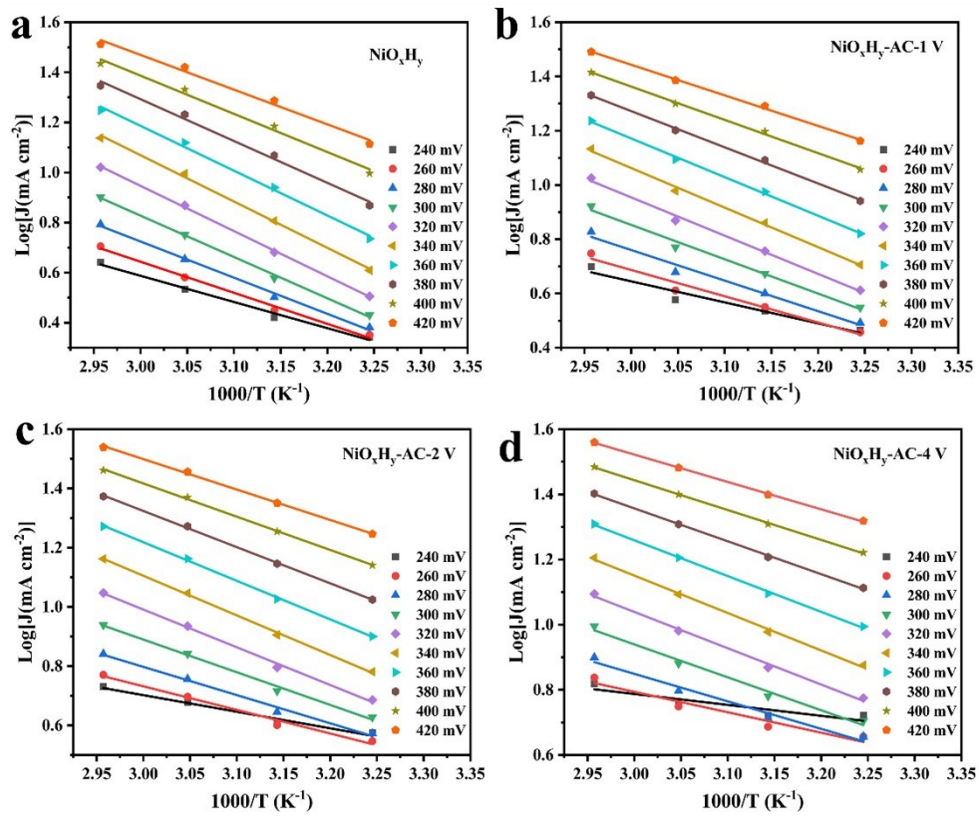
Fig. S20 Log(j) plotted against 1000/T (a). NiO$_x$H$_y$ (b). NiO$_x$H$_y$-AC-1V (c). NiO$_x$H$_y$-AC-2V (d). NiO$_x$H$_y$-AC-4V.

Table S1. EIS fitting data of NiO_xH_y. η is overpotential.

η (mV)	R_1 (Ω)	R_{int} (Ω)	CPE_1-T ($F^{-1} \cdot s^{1-n}$)	CPE_1-P	R_{ct} (Ω)	CPE_2-T ($F^{-1} \cdot s^{1-n}$)	CPE_2-P
340	3.169	0.802	0.150	0.541	10.7	0.0690	0.909
360	3.18	0.464	0.0701	0.633	6.495	0.0654	0.884
380	3.189	0.383	0.0506	0.666	4.316	0.0642	0.874
400	3.205	0.332	0.0370	0.700	3.176	0.0626	0.869
420	3.216	0.342	0.0389	0.687	2.529	0.0612	0.878

Table S2. EIS fitting data of NiO_xH_y-1 V.

η (mV)	R_1 (Ω)	R_{int} (Ω)	CPE_1-T ($F^{-1} \cdot s^{1-n}$)	CPE_1-P	R_{ct} (Ω)	CPE_2-T ($F^{-1} \cdot s^{1-n}$)	CPE_2-P
300	3.122	57.3	0.394	0.364	37.39	0.101	0.942
320	3.162	3.194	0.293	0.405	18.44	0.0871	0.924
340	3.18	0.942	0.182	0.453	9.64	0.0765	0.875
360	3.194	0.427	0.0546	0.598	6.497	0.0732	0.817
380	3.205	0.374	0.0394	0.635	5.02	0.0715	0.807

Table S3. EIS fitting data of NiO_xH_y-2 V.

η (mV)	R_1 (Ω)	R_{int} (Ω)	CPE_1-T $(F^{-1} \cdot s^{1-n})$	CPE_1-P	R_{ct} (Ω)	CPE_2-T $(F^{-1} \cdot s^{1-n})$	CPE_2-P
300	3.02	17.12	0.298	0.433	27.35	0.126	0.979
320	3.064	5.04	0.260	0.431	14.48	0.108	0.958
340	3.101	1.373	0.188	0.445	9.984	0.0879	0.890
360	3.114	0.756	0.112	0.492	6.762	0.0828	0.839
380	3.12	0.663	0.0955	0.499	5.081	0.0815	0.821

Table S4. EIS fitting data of NiO$_x$H$_y$-4 V.

η (mV)	R$_1$ (Ω)	R$_{int}$ (Ω)	CPE$_1$-T (F^{-1}·s^{1-n})	CPE$_1$-P	R$_{ct}$ (Ω)	CPE$_2$-T (F^{-1}·s^{1-n})	CPE$_2$-P
300	2.637	2.741	0.653	0.362	14.85	0.129	0.848
320	2.669	1.02	0.589	0.314	7.354	0.120	0.867
340	2.658	0.730	0.601	0.254	4.105	0.123	0.880
360	2.626	0.731	0.596	0.201	3.059	0.118	0.865
380	2.404	4.647	1.026	0.0761	2.317	0.112	0.884

Table S5. EIS fitting data of NiO_xH_y before and after SW-AC activation at different potentials.

		R_1 (Ω)	R_{int} (Ω)	CPE_1-T (F^{-1}·s^{1-n})	CPE_1-P	R_{ct} (Ω)	CPE_2-T (F^{-1}·s^{1-n})	CPE_2-P
Sample	NiO_xH_y	2.923	1.594	0.000401	0.558	19.04	0.0513	0.886
1	NiO_xH_y-AC-1 V	2.942	1.511	0.000482	0.552	15.79	0.0593	0.875
Sample	NiO_xH_y	2.513	1.619	0.0254	0.228	15.82	0.0676	0.907
2	NiO_xH_y-AC-2 V	2.966	0.976	0.0422	0.282	9.467	0.0831	0.892
Sample	NiO_xH_y	0.000211	11.07	0.155	0.0236	25.92	0.0405	0.9104
3	NiO_xH_y-AC-4 V	3.143	1.308	0.372	0.212	8.724	0.057	0.905

Table S6. Peaks position in Ni 2p XPS spectrum of NiO_xH_y and NiO_xH_y-AC-X.

Ni 2p	Satellite		Ni^{3+}		Ni^{2+}	
	position		position		position	
NiO_xH_y	877.90	859.58	871.94	854.42	870.02	852.68
NiO_xH_y-AC-1 V	878.7	859.86	871.98	854.82	869.64	852.96
NiO_xH_y-AC-2 V	878.58	860.04	872.04	854.52	869.82	852.54
NiO_xH_y-AC-4 V	878.63	860.15	872.51	854.57	870.89	852.77

Table S7. Peaks position in O 1s XPS spectrum of NiO_xH_y and NiO_xH_y-AC-X.

O 1s	Ni-OH position	V_O position	Ni-O position
NiO_xH_y	531.57	529.92	528.10
NiO_xH_y-AC-1 V	531.36	529.60	528.00
NiO_xH_y-AC-2 V	532.19	530.45	528.43
NiO_xH_y-AC-4 V	531.30	529.81	528.00

Table S8. Peaks position of Ni 2p XPS spectra of NiO_xH_y at different etching degree.

Ni 2p	Satellite		Ni^{3+}		Ni^{2+}		Ni^0	
	position		position		position		position	
10 nm	878.72	860.11	873.12	855.24	871.23	853.18	869.50	851.61
50 nm	877.96	860.15	873.36	855.32	871.35	853.43	869.46	852.06
100 nm	876.82	860.15	873.12	855.48	871.43	853.59	869.46	852.14

Table S9. Peaks position of Ni 2p XPS spectra of NiO_xH_y-AC-4 V at different etching degree.

Ni 2p	Satellite position		Ni^{3+} position		Ni^{2+} position		Ni^{0} position	
10 nm	878.68	860.35	873.81	855.32	871.79	853.22	869.86	851.65
50 nm	879.08	860.43	873.81	855.44	871.87	853.47	869.66	851.97
100 nm	878.31	860.47	873.81	855.56	871.83	853.55	869.58	852.06

Table S10. Peaks position of O 1s XPS spectra of NiO_xH_y at different etching degree.

O 1s	V_O position	Ni-O position
10 nm	530.81	529.08
50 nm	530.81	529.20
100 nm	530.81	529.30

Table S11. Peaks position of Ni 2p XPS spectra of NiO$_x$H$_y$-AC-4 V at different etching degree.

O 1s	V$_O$ position	Ni-O position
10 nm	530.84	529.00
50 nm	530.98	529.21
100 nm	531.03	529.28

REFERENCES

1   X. Li, M. Ahmadi, L. Collins and S. V. Kalinin, *Electrochim. Acta*, 2019, **313**, 570-583.
2   H. N. Nong, L. J. Falling, A. Bergmann, M. Klingenhof, H. P. Tran, C. Spori, R. Mom, J. Timoshenko, G. Zichittella, A. Knop-Gericke, S. Piccinin, J. Perez-Ramirez, B. R. Cuenya, R. Schlogl, P. Strasser, D. Teschner and T. E. Jones, *Nature*, 2020, **587**, 408-413.
3   C. I. Drexler, T. C. Miller, B. A. Rogers, Y. C. Li, C. A. Daly, Jr., T. Yang, S. A. Corcelli and P. S. Cremer, *J. Am. Chem. Soc.* , 2019, **141**, 6930-6936.
4   Y. Duan, N. Dubouis, J. Huang, D. A. Dalla Corte, V. Pimenta, Z. J. Xu and A. Grimaud, *ACS Catal.*, 2020, **10**, 4160-4170.
5   R. Zhang, W. Liu, F.-M. Zhang, Z.-D. Yang, G. Zhang and X. C. Zeng, *Appl. Catal., B*, 2023, **325**, 122366.
6   Y. Pan, X. Wang, W. Zhang, L. Tang, Z. Mu, C. Liu, B. Tian, M. Fei, Y. Sun, H. Su, L. Gao, P. Wang, X. Duan, J. Ma and M. Ding, *Nat. Commun.*, 2022, **13**, 3063.
7   R. Urrego-Ortiz, S. Builes and F. Calle-Vallejo, *ACS Catal.*, 2022, **12**, 4784-4791.